American Journal of Civil and Environmental Engineering
2018; 3(2): 19-36
http://www.aascit.org/journal/ajcee

AASCIT American Association for Science and Technology

Convective Energy Transmission Within a Porous Trapezoidal Enclosure Under Ascendancy of Magnetic Field with Linearly Heated/Cold Wall

Ziafat Mehmood*, Tariq Javed, Muhammad Arshad Siddiqui

Department of Mathematics and Statistics, International Islamic University, Islamabad, Pakistan

Email address

rajaziafat@yahoo.com (Z. Mehmood)

*Corresponding author

Citation

Ziafat Mehmood, Tariq Javed, Muhammad Arshad Siddiqui. Convective Energy Transmission Within a Porous Trapezoidal Enclosure Under Ascendancy of Magnetic Field with Linearly Heated/Cold Wall. *American Journal of Civil and Environmental Engineering.* Vol. 3, No. 2, 2018, pp. 19-36.

Received: February 23, 2018; **Accepted**: March 15, 2018; **Published**: April 27, 2018

Abstract: The present article comprises a numerical analysis of free convection heat transfer inside a porous trapezoidal container influenced by MHD when bottom wall is subject to uniform temperature profile, left wall is provided with linear heating, right wall is taken either cold or linearly heated and upper wall is perfectly insulated. Momentum and energy equations describing the flow problem are modeled and exposed first to Penalty method to remove pressure term from momentum equations and afterwards reduced equations are solved by incorporating the Galerkin weighted residual method. Computed solutions are presented through curves for streamlines, isotherms and local heat transfer rate for various values of involved parameters including Prandtl number Pr ($0.026 \leq Pr \leq 1000$), Hartman number Ha ($50 \leq Ha \leq 1000$) and Darcy number Da ($10^{-5} \leq Da \leq 10^{-3}$) where, Rayleigh number Ra is fixed at 106, considering three different cases of cavity, in which inclination of side walls of enclosure is taken to be 0, 30 and 45 degrees. This inquisition showed that the strength of streamline circulations escalates when Darcy and Prandtl numbers are amplified where, symmetric isotherms and streamlines are observed in case of non-uniform heating for tilt angles 30 and 45 degrees where due to conduction dominance smooth and monotonic isotherms are seen for small Darcy number but increasing Darcy number results in distorted isotherm contours indicating dominance of convection regime.

Keywords: Natural Convection, Penalty Method, Finite Element Method (FEM), Cavity Flow

1. Introduction

Heat transfer in cavity flow has successfully grabbed attention of investigators in recent years as it has numerous applications in engineering and different chemical processes. Food items are undergone through natural convection during their shelf life especially in domestic refrigerator where they spend most of their shelf life. Natural convection and airflow in a refrigerator occurs due to the variation in air density which is dependent upon temperature gradient. Furthermore, natural convection is also involved in applications such as electronic equipment cooling, fire research and solar thermal conversion etc. Heat transfer is involved in heating and cooling of batch tanks, Heat Exchangers, Condensers, Boilers & Calandrias, Evaporators etc. Whereas, lid-driven cavity flows help to analyse flow properties in complex close region with recirculation, e.g. coating rolls, contracting flow and flows on slit are of soul importance in various applications like coater for short-dwell and flexible blades.

Recently extensive research has been carried out on free convection heat transmission within containers of different geometries. In particular porous trapezoidal cavity has grabbed the interest of many investigators due to its vast engineering applications. Basak et al. [1] investigated phenomena of convective heat flow inside a trapezoidal container by computing results against different inclination angles of inclined boundaries when horizontal lower wall is heated uniformly and non-uniformly. He obtained results for several values of Darcy number ranging 10^{-5} to 10^{-3}. Varol et al. [2] expressed computational solutions for free convection through porous cavity of rectangular shape, considering effects of sinusoidal heat at bottom wall. He applied finite difference scheme to get numerical solutions and showed computations

for different ranges of aspect ratio AR ($0.25 \leq AR \leq 1.0$) and amplitude λ of sinusoidal wave at bottom ($0.25 \leq \lambda \leq 1.0$). Bejan and Poulikakos [3] discussed energy flow through free convection through porous medium within a vertical layer considering non Darcian regime. Basak et al. [4] examined heat flow through porous media contained in a square container and calculated numerical results when bottom boundary is provided heat uniformly and uniformly where upper wall is insulted and vertical boundaries are cold. Streamlines and isotherms are expressed for various Rayleigh, Prandtl and Darcy numbers. Chen et al. [5] considered Darcy-Brinkman-Forchheimer extended model in order to investigate numerical simulations for convective heat flow through wavy container considering isothermal vertical boundaries, where horizontal boundaries are insulated. He computed solutions for different values of parameters including wave ratio λ ($0 \leq \lambda \leq 1.8$) aspect ratio A ($1 \leq A \leq 5$) and Darcy number Da ($10^{-6} \leq Da \leq 10^{-1}$). Simulations for heat transfer with different inclination angles through a trapezoidal cavity when linear heating is provided to inclined walls and uniform heating is provided to bottom wall is carried out by Basak et al. [6]. An investigation on heat flow in porous trapezoidal cavity under the effects of various walls heating was also done by Basak et al. [7]. He used penalty approach to compute numerical solutions and presented numerical simulations for different tilt angles ($\phi = 0^o, 30^o, 45^o$) and verity of values for different parameters. Anandalakshmi and Basak [8] presented an investigation on heat flow visualization for free convective heat flow in rhombic enclosure where bottom boundary of cavity is subject to constant and variable heating profile. Khashan et al. [9] numerically investigated energy transmission within porous enclosure using non-Darcian and thermal non-equilibrium model when bottom wall is isothermal. They applied FVM to compute numerical results for governing Navier Stoke's equations and plotted curves for various values of involved parameters e.g. Rayleigh number $Ra = 1 - 400$, Darcy number $Da = 10^{-4} - 10^{-3}$, thermal conductivity ratio of fluid and solid $\kappa = 0.1 - 1.0$ and modified Biot number $\chi = 1 - 100$. Poulikakos and Bejan [10] carried out a study of energy flow inside vertical porous layer using Darcy–Forchheimer model.

Merrikh and Mohamad [11] discussed Non-Darian effect on buoyancy flow through a cavity containing two vertical layers of porous medium. They focused on legitimacy of Darcy model for several combinations of Permeability ratio, Rayleigh and Darcy numbers. Unsteady natural convection within porous cavity by means of two energy model is studied by Al-Amiri [12] and numerical simulations were presented for numerous values of Grashof number $Gr = 10^4 - 10^6$ and Darcy number $Da = 10^{-5} - 10^{-1}$. Lauriat and Prasad [13] considered Darcy-Brinkman-Forchheimer model and analyzed heat flow through vertical porous enclosure. Forced convective energy flow inside a channel having 16 porous baffles is discussed by Miranda and Anand [14]. Kim et al. [15] discussed phenomena of buoyant convection with heat generating porous media with the help of extended Brinkman-Darcy model within a square container. Basak et al. [16] presented energy flow by free convection numerically through porous trapezoidal container heated constantly and variably from lower boundary and plotted graphs for wide ranges of parameters involving Rayleigh, Prandtl and Darcy numbers. Computations for convective energy flow inside a porous enclosure of trapezoidal shape with different tilt angles ($\phi = 0^o, 30^o, 45^o$) and uniformly/non-uniformly heated lower boundary against Rayleigh number Ra ranging ($10^3 \leq Ra \leq 10^6$) are also presented by Basak et al. [17]. Basak et al. [18] has also investigated numerical simulations based on heatline concept heat flow in a trapezoidal enclosure tilted at different angles ($\phi = 0^o, 30^o, 45^o$) when bottom boundary of cavity is provided uniform or nonuniform heat where insulated top boundary and cold side boundries are considered.

Hossain and Alim [19] studied trapezoidal cavity with MHD effects and non-uniformly heated lower boundary. Basak et al. [20] investigated thermal boundary condition's effects heat transfer through a square enclosure considering various heating profiles. He used penalty method to compute numerical results for different ranges of Rayleigh and Prandtl numbers. Moallemi and Jang [21] carried out numerical study for influence of Prandtl number on mix-convective energy flow through a lid-driven square enclosure considering heated bottom wall. Numerical analysis of free convection energy flow inside a square container provided heat non-uniformly is done by Roy and Basak [22] against numerous values of Rayleigh and Prandtl numbers. Basak et al. [23] conveyed an investigation on mixed convective energy transfer analysis within square cavity when lower horizontal boundary is subject to constant and variable heat for verity of Grashof number Gr ($10^3 \leq Gr \leq 10^5$).

In addition to above mentioned studies there are several experimental investigations exploring the features of heat and fluid flow inside the cavities of various geometrical shapes for the engineering and industrial importance of heat transfer in cavity flows. Lee [24] experimentally and computationally investigated convective energy flow through a trapezoidal container containing incompressible fluid having side walls inclination of 45 degree. He performed the experiment to study influence of Rayleigh number, positioning and aspect ratio on flow structure using smoke to visualize the flow regime. Lee [25] also conveyed a study on numerical experiments with convection in trapezoidal cavity to analyse the influence of Prandtl & Rayleigh numbers, different wall angles and various orientation angles on the energy flow. Iyican et al. [26] showed an experimental analysis of natural convection inside a trapezoidal enclosure against various values of Rayleigh number and varying tilt angles. Eyden et al. [27] conveyed experimental results to analyse double diffusive free convection through trapezoidal container filled with fusion of a couple of gases to mimic idealised situation in underground coal gasification. Hu et al. [28] experimentally and computationally examined energy flow through a square container having aluminium-water nanofluid and showed considerable agreement between experimental and numerical results. Similarly there are many [29-33] experimental studies investigating the energy flow in containers of different geometries under different conditions for having numerous engineering and industrial applications

including so-called moderately concentrating solar collector, a transonic cascade and turbo-machinery etc.

Motivated from above reviewed literature porous trapezoidal cavity is investigated in this manuscript for natural convection in presence of MHD, which has not been investigated yet as per author's best knowledge. Here we have considered uniform heating along bottom wall, linear heating along left wall, perfectly insulated upper wall and for right wall we have considered two cases, (i) cold, (ii) linear heated. Results are described in the form of contours against several values of Prandtl number Pr ($0.026 \le Pr \le 1000$), Rayleigh number Ra ($10^3 \le Ra \le 10^6$), Darcy number Da ($10^{-5} \le Da \le 10^{-3}$) and Hartman number Ha ($50 \le Ha \le 1000$).

2. Mathematical Model

An electrically conducting laminar flow of incompressible viscous fluid through a trapezoidal enclosure containing isotropic porous medium has been considered in this investigation as shown in Figure 1. Local thermal equilibrium has been considered between solid matrix and voids inside the porous region. All physical parameters are assumed constant excluding density which is function of temperature. Variation in density causes a body force term in momentum equation after applying Boussinesq approximation [34]. Furthermore, constant magnetic field B with uniform magnitude B_0 is considered along x-axis which gives rise to the Lorentz force $f = j \times B$. The mathematical form of Ohm's Law is $j = \sigma(E + u \times B)$ where u is velocity and E is electric field. Since quasi-static approximation is assumed in our study therefore induced magnetic field is negligible and the field is completely given by the imposed field B. in this case $\nabla \times E = 0$ and charge conservation equation $\nabla . j = 0$ may be exploited to eliminate current density j from Ohm's Law. In contrast to the full MHD equation the system only contains one electromagnetic variable. Finally the Lorentz force is reduced to $f = (u \times B) \times B$ which depends linearly on velocity and qudratically on strength of magnetic field as expressed in Eq. (3) [see Ref. 35]. Here induced magnetic field is neglected being small enough in comparison of B_0 (low-R_m approximation [36]). We neglect joule effects and viscous dissipation while all walls of enclosure are considered electrically insulated with no Hall effects. Incorporating above mentioned assumptions following are mass, momentum and energy balance equations governing flow problem.

$$\frac{\partial u}{\partial x}+\frac{\partial v}{\partial y}=0, \tag{1}$$

$$u\frac{\partial u}{\partial x}+v\frac{\partial u}{\partial y}=-\frac{1}{\rho}\frac{\partial p}{\partial x}+\upsilon\left(\frac{\partial^2 u}{\partial x^2}+\frac{\partial^2 u}{\partial y^2}\right)-\frac{\upsilon}{K}u, \tag{2}$$

$$u\frac{\partial v}{\partial x}+v\frac{\partial v}{\partial y}=-\frac{1}{\rho}\frac{\partial p}{\partial y}+\upsilon\left(\frac{\partial^2 v}{\partial x^2}+\frac{\partial^2 v}{\partial y^2}\right)-\frac{\upsilon}{K}v+g\beta\left(T-T_c\right)-\frac{\sigma B_o^2}{\rho}v, \tag{3}$$

and

$$u\frac{\partial T}{\partial x}+v\frac{\partial T}{\partial y}=\alpha\left(\frac{\partial^2 T}{\partial x^2}+\frac{\partial^2 T}{\partial y^2}\right). \tag{4}$$

subject to boundary conditions

$$\begin{aligned}
&u(x,0)=v(x,0)=0, T(x,0)=T_h,\\
&u(x,L)=0, v(x,L)=0, \frac{\partial T(x,L)}{\partial y}=0,\\
&u=0, v=0, T=1-y \ at \ x\sin\phi+y\cos\phi=0 \text{ and } 0\le y\le L,\\
&u=0, v=0, T=1-y \text{ or } 0 \ at \ x\sin\phi-y\cos\phi=\cos\phi \text{ and } 0\le y\le L.
\end{aligned} \tag{5}$$

Where x, y represents rectangular coordinates, u, v shows components of velocity filed in horizontal and vertical direction, P is pressure, υ is kinematic viscosity and ρ is density. We define following dimensionless variables to non-dimensionalize the above Eqns.

$$\begin{aligned}
&X=\frac{x}{L}, Y=\frac{y}{L}, U=\frac{uL}{\alpha}, V=\frac{vL}{\alpha}, P=\frac{pL^2}{\rho\alpha^2},\\
&\theta=\frac{T-T_c}{T_h-T_c}, \Pr=\frac{\nu}{\alpha}, Gr=\frac{g\beta L^3\left(T_h-T_c\right)}{\nu^2}, Da=\frac{\upsilon}{K}\\
&Ra=\frac{g\beta L^3\left(T_h-T_c\right)\Pr}{\nu^2}, Ha^2=\frac{\sigma {B_o}^2 L^2}{\mu}, \alpha=\frac{k}{\rho C_p}
\end{aligned} \tag{6}$$

substituting (6) in (1)-(4) we get

$$\frac{\partial U}{\partial X}+\frac{\partial V}{\partial Y}=0 \tag{7}$$

$$U\frac{\partial U}{\partial X}+V\frac{\partial U}{\partial Y}=-\frac{\partial P}{\partial X}+\Pr\left(\frac{\partial^2 U}{\partial X^2}+\frac{\partial^2 U}{\partial Y^2}\right)-\frac{\Pr}{Da}U \tag{8}$$

$$U\frac{\partial V}{\partial X}+V\frac{\partial V}{\partial Y}=-\frac{\partial P}{\partial Y}+\Pr\left(\frac{\partial^2 V}{\partial X^2}+\frac{\partial^2 V}{\partial Y^2}\right)-\frac{\Pr}{Da}V+RaPr\theta-Ha^2PrV \tag{9}$$

$$U\frac{\partial \theta}{\partial X}+V\frac{\partial \theta}{\partial Y}=\frac{\partial^2 \theta}{\partial X^2}+\frac{\partial^2 \theta}{\partial Y^2} \tag{10}$$

Under the following boundary conditions

$$\begin{aligned}&U(X,0)=V(X,0)=0,\theta(X,0)=1.\\&U(X,1)=0=V(X,1),\frac{\partial\theta(X,1)}{\partial Y}=0.\\&U=0=V,\theta=1-Y\ at\ \mathrm{X}\sin\phi+Y\cos\phi=0\ \text{and}\ 0\le Y\le 1\\&U=V=0,\theta=1-Y\ \text{or}\ 0\ at\ \mathrm{X}\sin\phi-Y\cos\phi=\cos\phi\ \text{and}\ 0\le Y\le 1\end{aligned} \tag{11}$$

Here *U, V* corresponds to dimensionless components of velocity, θ is dimensionless temperature, *Pr, Ra, Gr, Ha* and *Da* are Prandtl, Rayleigh, Grashof, Hartman and Darcy numbers respectively.

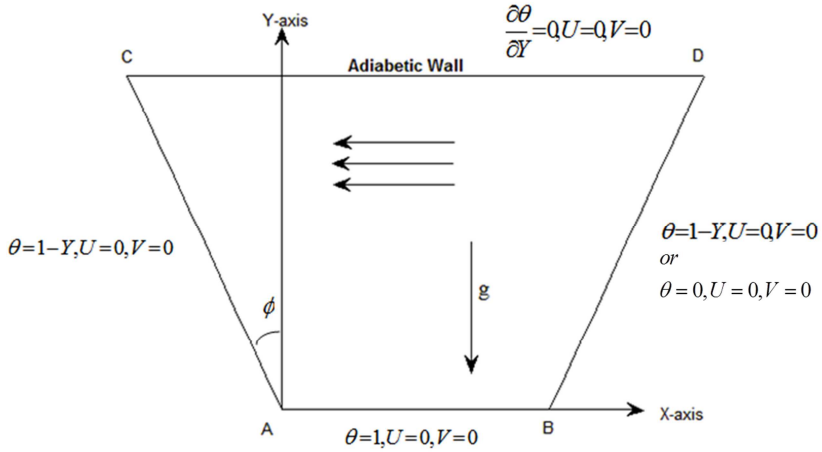

Figure 1. *Trapezoidal cavity flow with various heated walls.*

Energy flow rate is determined the form of local Nusselt numbers *Nu,* defined as

$$Nu=-\frac{\partial\theta}{\partial n} \tag{12}$$

3. Method of Solution

Penalty method is incorporated to deal with pressure term appearing in momentum equation with the help of continuity equation [37]-[39]. Afterwards the simplified equations are solved through Galerkin weighted residual scheme. Following incompressibility condition is defined by introducing penalty parameter γ.

$$P=-\gamma\left(\frac{\partial U}{\partial X}+\frac{\partial V}{\partial Y}\right) \tag{13}$$

To satisfy continuity equation we have to take large value for γ, generally γ=10^7 returns consistent results. Using Eq. (13), momentum equations become

$$U\frac{\partial U}{\partial x}+V\frac{\partial U}{\partial y}=\gamma\frac{\partial}{\partial X}\left(\frac{\partial U}{\partial X}+\frac{\partial V}{\partial Y}\right)+\Pr\left(\frac{\partial^2 U}{\partial x^2}+\frac{\partial^2 U}{\partial y^2}\right)-\frac{\Pr}{Da}U \tag{14}$$

and

$$U\frac{\partial V}{\partial x}+V\frac{\partial V}{\partial y}=\gamma\frac{\partial}{\partial Y}\left(\frac{\partial U}{\partial X}+\frac{\partial V}{\partial Y}\right)+\Pr\left(\frac{\partial^2 V}{\partial x^2}+\frac{\partial^2 V}{\partial y^2}\right)-\frac{\Pr}{Da}V+RaPr\theta-Ha^2PrV \tag{15}$$

We estimate the velocity components and temperature profile through 6-nodal triangular elements with bi-quadratic basis functions $\{\phi_k\}_{k=1}^{N}$ as follows.

$$U\approx\sum_{k=1}^{N}U_k\phi_k(X,Y),V\approx\sum_{k=1}^{N}V_k\phi_k(X,Y),\theta\approx\sum_{k=1}^{N}\theta_k\phi_k(X,Y). \tag{16}$$

following residual expressions of above equations are reduced by incorporating Galerkin scheme of finite element method for internal domain Ω

$$\begin{aligned}R_i^1=&\sum_{k=1}^{N}U_k\int_{\Omega}\left[\left(\sum_{k=1}^{N}U_k\phi_k\right)\frac{\partial\phi_k}{\partial X}+\left(\sum_{k=1}^{N}V_k\phi_k\right)\frac{\partial\phi_k}{\partial Y}\right]\phi_i dXdY\\&+\gamma\left[\sum_{k=1}^{N}U_k\int_{\Omega}\frac{\partial\phi_i}{\partial X}\frac{\partial\phi_k}{\partial X}dXdY+\sum_{k=1}^{N}V_k\int_{\Omega}\frac{\partial\phi_i}{\partial X}\frac{\partial\phi_k}{\partial Y}dXdY\right]\\&+\Pr\sum_{k=1}^{N}U_k\int_{\Omega}\left[\frac{\partial\phi_i}{\partial X}\frac{\partial\phi_k}{\partial X}+\frac{\partial\phi_i}{\partial Y}\frac{\partial\phi_k}{\partial Y}\right]dXdY+\frac{\Pr}{Da}\int_{\Omega}\left[\sum_{k=1}^{N}U_k\phi_k\right]\phi_i dXdY\end{aligned} \tag{17}$$

$$\begin{aligned}R_i^2=&\sum_{k=1}^{N}V_k\int_{\Omega}\left[\left(\sum_{k=1}^{N}U_k\phi_k\right)\frac{\partial\phi_k}{\partial X}+\left(\sum_{k=1}^{N}V_k\phi_k\right)\frac{\partial\phi_k}{\partial Y}\right]\phi_i dXdY\\&+\gamma\left[\sum_{k=1}^{N}U_k\int_{\Omega}\frac{\partial\phi_i}{\partial Y}\frac{\partial\phi_k}{\partial X}dXdY+\sum_{k=1}^{N}V_k\int_{\Omega}\frac{\partial\phi_i}{\partial Y}\frac{\partial\phi_k}{\partial Y}dXdY\right]\\&+\Pr\sum_{k=1}^{N}V_k\int_{\Omega}\left[\frac{\partial\phi_i}{\partial X}\frac{\partial\phi_k}{\partial X}+\frac{\partial\phi_i}{\partial Y}\frac{\partial\phi_k}{\partial Y}\right]dXdY+\frac{\Pr}{Da}\int_{\Omega}\left[\sum_{k=1}^{N}V_k\phi_k\right]\phi_i dXdY\\&-Ra\Pr\int_{\Omega}\left[\sum_{k=1}^{N}\theta_k\phi_k\right]\phi_i dXdY-Ha^2\Pr\int_{\Omega}\left[\sum_{k=1}^{N}V_k\phi_k\right]\phi_i dXdY\end{aligned} \tag{18}$$

$$\begin{aligned}R_i^3=&\sum_{k=1}^{N}\theta_k\int_{\Omega}\left[\left(\sum_{k=1}^{N}U_k\phi_k\right)\frac{\partial\phi_k}{\partial X}+\left(\sum_{k=1}^{N}V_k\phi_k\right)\frac{\partial\phi_k}{\partial Y}\right]\phi_i dXdY\\&+\sum_{k=1}^{N}\theta_k\int_{\Omega}\left[\frac{\partial\phi_i}{\partial X}\frac{\partial\phi_k}{\partial X}+\frac{\partial\phi_i}{\partial Y}\frac{\partial\phi_k}{\partial Y}\right]dXdY\end{aligned} \tag{19}$$

Solution of nonlinear residual equations (17)-(19) are iteratively obtained with the help of Newton Raphson method. The flow is determined through stream function defined using velocity components as follows

$$U=\frac{\partial\psi}{\partial Y},\ \text{and}\ \ V=-\frac{\partial\psi}{\partial X} \tag{20}$$

Following single equation may be obtained from above

$$\frac{\partial^2\psi}{\partial X^2}+\frac{\partial^2\psi}{\partial Y^2}=\frac{\partial U}{\partial Y}-\frac{\partial V}{\partial X} \tag{21}$$

stream functions are also approximated by same basis functions $\{\phi_k\}_{k=1}^{N}$ as

$$\psi\approx\sum_{k=1}^{N}\psi_k\phi_k(X,Y) \tag{22}$$

and after applying Galerkin weighted residual technique residual equation for stream function take the following form and it is further solved with no-slip boundary conditions along all the boundaries

$$R_i^s = \sum_{k=1}^{N} \psi_k \int_{\Omega} \left[\frac{\partial \phi_i}{\partial X} \frac{\partial \phi_k}{\partial X} + \frac{\partial \phi_i}{\partial Y} \frac{\partial \phi_k}{\partial Y} \right] dXdY + \sum_{k=1}^{N} U_k \int_{\Omega} \phi_i \frac{\partial \phi_k}{\partial Y} dXdY - \sum_{k=1}^{N} V_k \int_{\Omega} \phi_i \frac{\partial \phi_k}{\partial X} dXdY \tag{23}$$

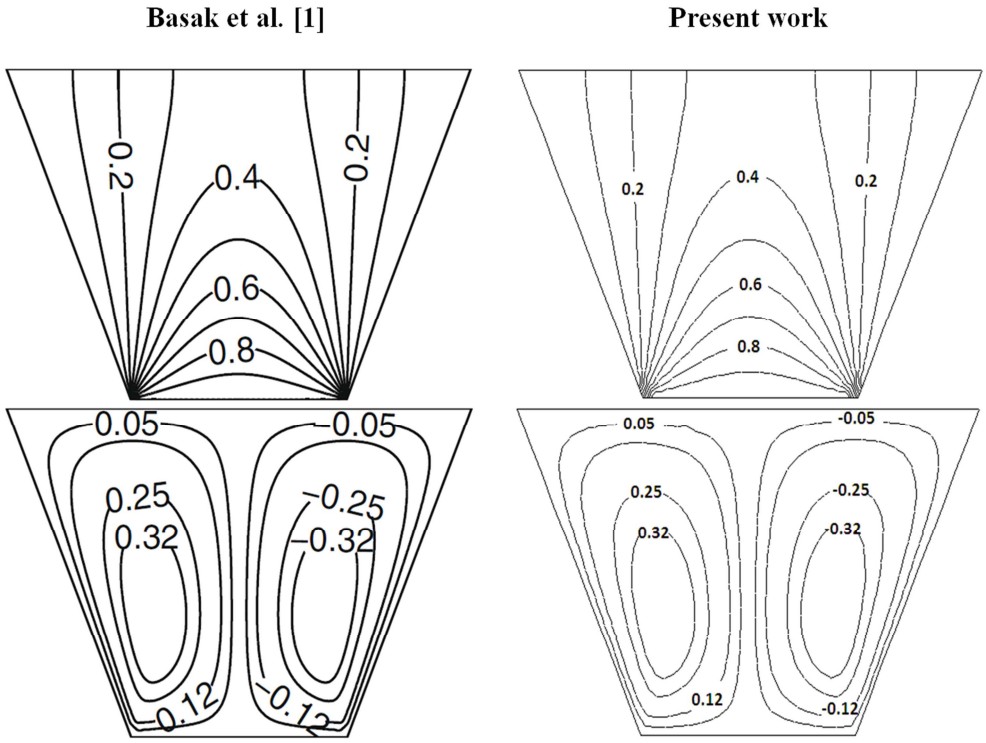

Figure 2. *Streamlines and isotherms for Pr =7.2, Ra =* 10^6 *and Da =* 10^{-5}.

4. Validation

With objective to ensure accuracy of the code, developed to solve governing flow problem, we tested it against results of Basak et al. [1] for heat transfer through free convective heat transfer in porous trapezoidal enclosure as a limiting case for uniform heated bottom wall with Pr =7.2, Ra =10^6 and Da = 10^{-5}. Computations of our code are in good agreement with those of Basak et al. [1] as shown in Figure 2. In Figure 2 the results of Basak et al. [1] are shown in left column and results obtained by present investigation are shown in right column for comparison.

5. Results and Discussions

This section contains computational results for free convective heat flow through a porous trapezoidal enclosure under MHD effects. Our discussion is divided into two cases (i) cold and (ii) linearly heated right wall, where bottom wall is taken at uniform heating profile and upper boundary is considered insulated. Additionally heat flow rate in form of local Nusselt number are also presented and discussed in this section. Furthermore the solutions are shown for a wide ranges of pertinent flow parameters including Prandtl number Pr ($0.26 \leq Pr \leq 10^3$), Da ($10^{-5} \leq Da \leq 10^{-3}$) and Hartman Number Ha ($50 \leq Ha \leq 10^3$) where Rayleigh number is fixed at $Ra = 10^6$.

5.1. Cold Wall Case

In this case bottom wall is subject to a uniform heating, top wall is perfectly insulated, left wall is heated linearly and right wall is taken at zero temperature due to which there appears jump type discontinuity at the lower right corner as two walls meeting at that corner are at different temperatures. Computational singularity at this corner needs special treatment. One way to deal with this singularity is suggested by Ganzarolli and Milanez [40]. According to them corner node may be taken at average of bottom and side wall temperatures and adjacent nodes are kept on corresponding wall temperature to avoids singularity.

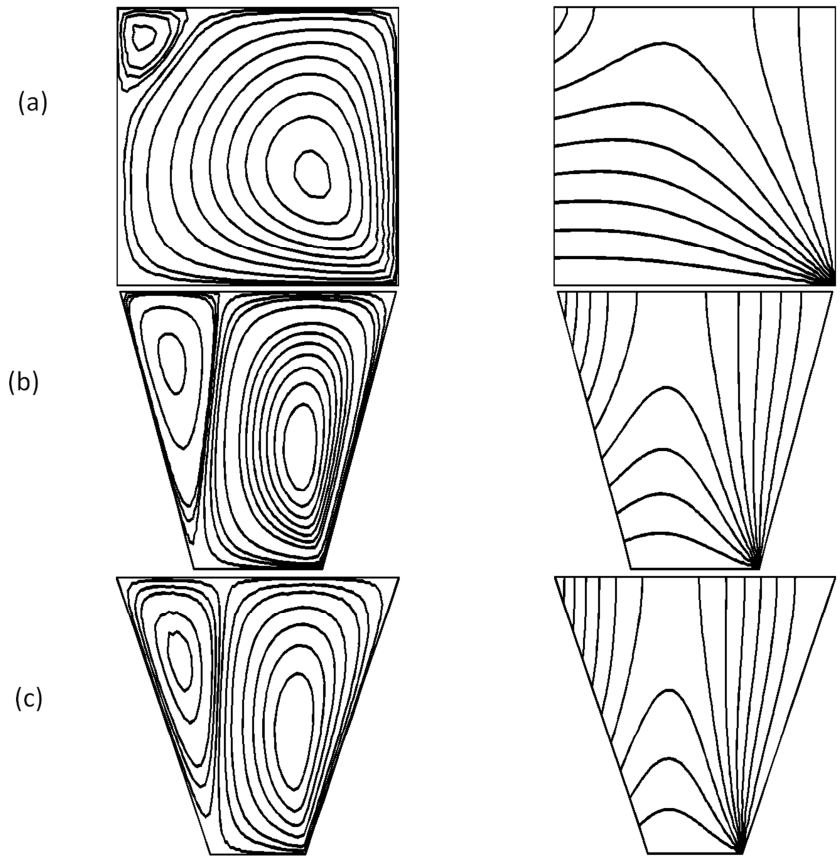

Figure 3. *Stream lines and Isotherms for cold right wall with* $Ra = 10^6, Pr = 0.026, Da = 10^{-5}$ *and* $Ha = 50$ *where (a)* $\phi = 0^o$ *(b)* $\phi = 30^o$ *(c)* $\phi = 45^o$.

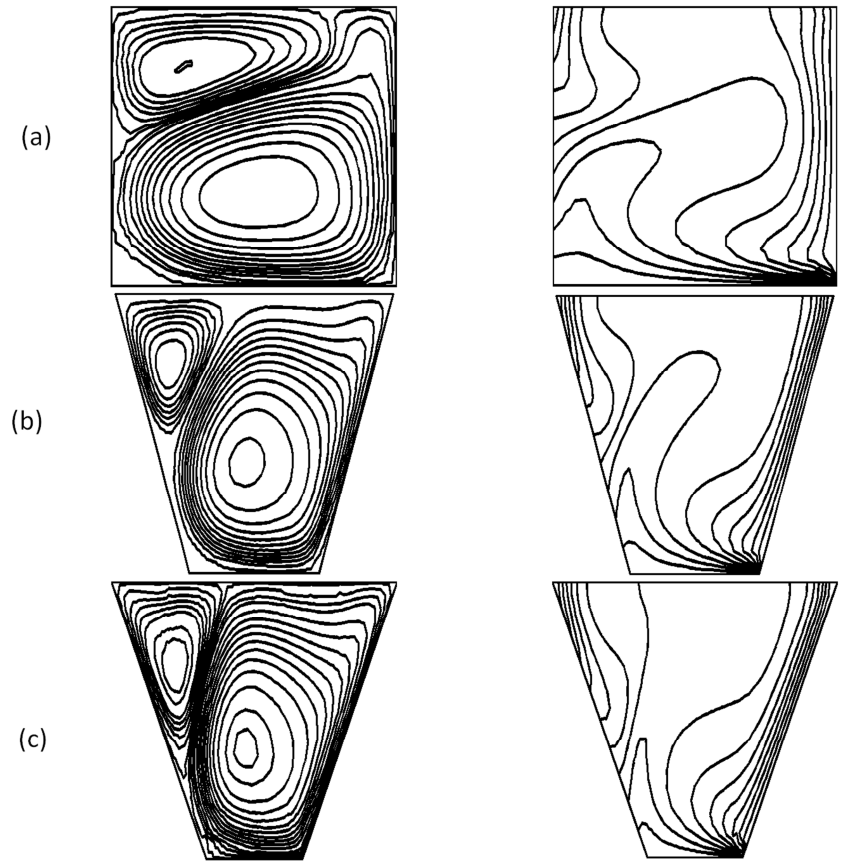

Figure 4. *Streamlines and Isotherms for cold right wall with* $Ra = 10^6, Pr = 0.026, Da = 10^{-3}$ *and* $Ha = 50$ *where (a)* $\phi = 0^o$ *(b)* $\phi = 30^o$ *(c)* $\phi = 45^o$.

Figures 3 and 4 illustrate contour plots for streamlines and isotherms with $Ra = 10^6, Da = 10^{-5} - 10^{-3}$ and $Ha = 50$. In Figure 3, isotherms appear to be smooth and monotonic showing conduction dominant regime. Whereas, for $\theta < 0.3$ when $\phi = 0$, for $\theta < 0.6$ when $\phi = 30^o$ and for $\theta < 0.7$ when $\phi = 45^o$, isotherms are broken-up to side walls. Simultaneously, weak anti-clockwise secondary circulation of stream lines is observed near upper left side of the cavity, in addition to primary clockwise circulation appearing in right portion of cavity. Where Maximum height of stream function ($|\psi|_{\max}$) is noted to be 0.5, 0.55 and 0.6 for $\phi = 0^o, 30^o$ and 45^o respectively. Figure 4 indicates that with increase in Darcy number *Da,* convection heat transfer becomes dominant and consequently, non-monotonic, non-symmetric and distorted isotherms are observed in this case. Furthermore, isotherms are accumulated to right wall while in lower half of the cavity, isotherms are pushed a little towards the left wall. On the other hand, stream lines appear as two oval rolls of anti-clockwise (upper left) and clockwise (lower right) circulations. Here, upper left secondary circulation also gets stronger with increase in Darcy number but clockwise primary circulation remains of more intensity as compared to secondary circulation, and is directed towards the right lower corner due to the singularity appearing at that corner. Where, maximum height of stream function in this case is noted to be 11.5, 11.8, and 12.5 for $\phi = 0^o, 30^o$ and 45^o respectively.

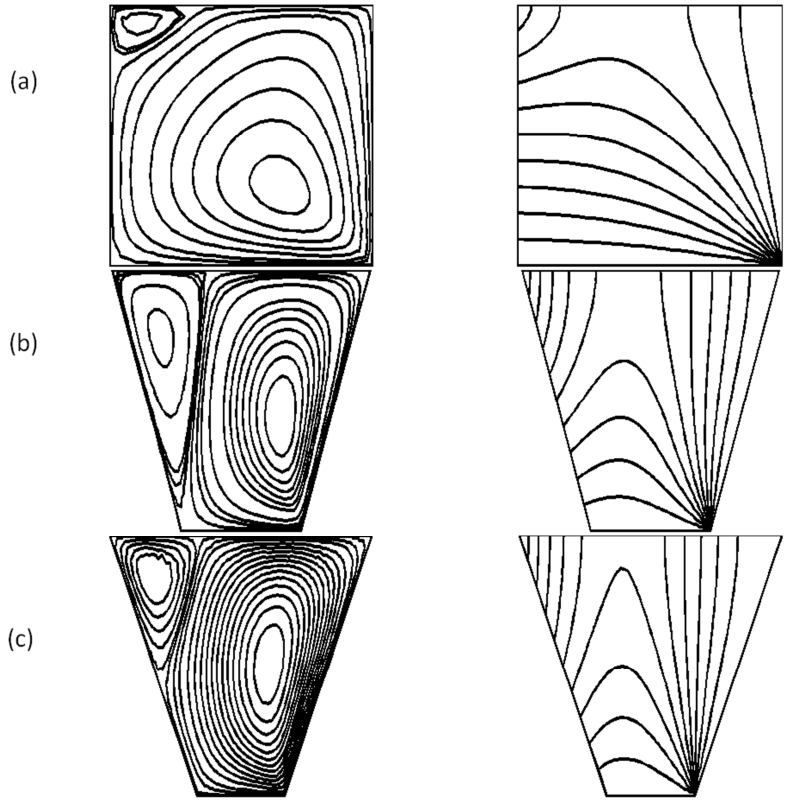

Figure 5. *Stream lines and Isotherms for cold right wall with* $Ra = 10^6, Pr = 0.7, Da = 10^{-5}$ *and* $Ha = 1000$ *where (a)* $\phi = 0^o$ *(b)* $\phi = 30^o$ *(c)* $\phi = 45^o$.

Figures 5-8 contains plots for $Ra = 10^6, Pr = 0.7 - 1000, Da = 10^{-5} - 10^{-3}$ and $Ha = 50$. It is observed that increase in Prandtl number, increases strength of both clockwise and anti-clockwise circulations and maximum heights of stream functions are noted to be 0.5, 0.55 and 0.6 for $\phi = 0^o, 30^o \; and \; 45^o$ respectively (Figure 5). It is further noted that, anti-clockwise circulations move downward along left wall with increase in tilt angle ϕ (see Figure 5). When Darcy number is raised to 10^{-3}, roll of anti-clockwise circulation is pinched into clockwise circulation appearing bottom right side and maximum height of streamlines is boosted to 11.5, 11.8, and 12.5 for $\phi = 0^o, 30^o \; and \; 45^o$ respectively as shown in Figure 6. Whereas, isotherms become monotonic for $\theta \geq 0.3$ when $\phi = 0^o$ (see Figure 5 a), while, for $\phi = 30^o$ and $\phi = 45^o$ curves are pushed upward along left wall when $\theta \geq 0.6$ (Figure 5 b, c). Whereas when Darcy number is amplified, isotherms are broken non-symmetrically and clustered to inclined walls of enclosure for $\theta \leq 0.6$ when $\phi = 0^o$, for $\theta \leq 0.7$ when $\phi = 30^o$, and $\theta \leq 0.8$ when $\phi = 45^o$ respectively as shown in Figure 6. Similar effects on isotherms and streamlines are observed when Prandtl number is mounted to 1000 while maximum heights of stream function are 0.5, 0.65 and 0.75 for $\phi = 0^o, 30^o \; and \; 45^o$ when $Da = 10^{-5}$ and 12.75, 14, 15.5 for $\phi = 0^o, 30^o \; and \; 45^o$ when $Da = 10^{-3}$ as exhibited in Figures 7 and 8.

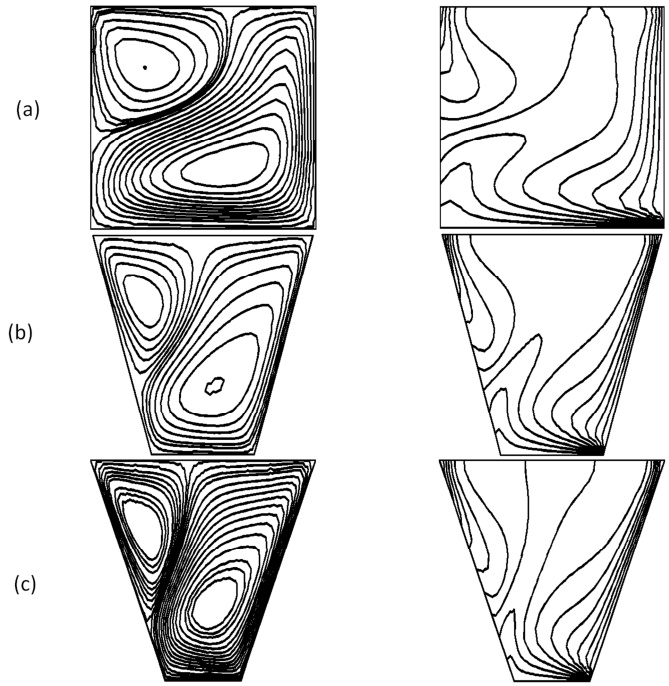

Figure 6. *Streamlines and Isotherms for cold right wall with* $Ra = 10^6, Pr = 0.7, Da = 10^{-3}$ *and* $Ha = 50$ *where (a)* $\phi = 0^o$ *(b)* $\phi = 30^o$ *(c)* $\phi = 45^o$.

5.2. Linearly Heated Wall

In this case both side walls are subjected to linearly varying heat profile and bottom wall is considered at uniform temperature while top wall is insulated. Considering this type of heating profile at right wall has an advantage, that it removes singularity from the bottom right corner.

In Figures 9, 10 contours plots are presented for stream function and isotherms against $Ra = 10^6, Pr = 0.026, Da = 10^{-5} - 10^{-3}$ and $Ha = 50$. It is delineated that, fluid goes up from the middle portion of uniformly heated bottom wall and comes down near linearly heated side walls forming two rolls of symmetric circulations about the vertical line passing from centre of enclosure. Here less intensive flow is seen for low Darcy number ($Da = 10^{-5}$) and centres of circulations move downwards to bottom wall with increase in tilt angle ϕ, while maximum heights of streamline circulations are noted to be 0.085, 0.18 and 0.2 for $\phi = 0^o, 30^o \; and \; 45^o$ respectively.

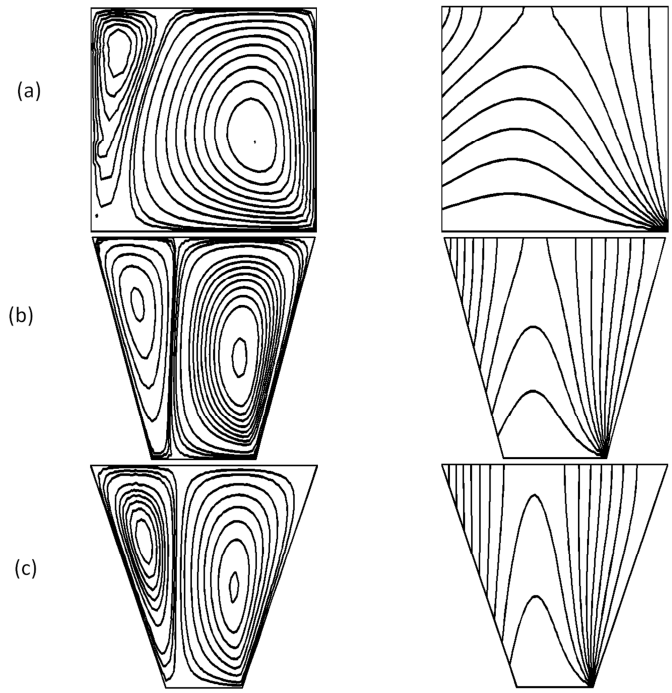

Figure 7. *Streamlines and Isotherms for cold right wall with* $Ra = 10^6, Pr = 10^3, Da = 10^{-5}$ *and* $Ha = 50$ *where (a)* $\phi = 0^o$ *(b)* $\phi = 30^o$ *(c)* $\phi = 45^o$.

On the other hand, in this case isotherms are also found symmetric about vertical line passing through centre of bottom and contours of isotherms are symmetrically broken up to side walls when $\theta \leq 0.3$ for $\phi = 0^o$ (square cavity), when $\theta \leq 0.6$ for $\phi = 30^o$ and when $\theta \leq 0.7$ for $\phi = 45^o$respectively as demonstrated in Figure 9.

When Darcy number is increased to 10^{-3}, three non-symmetric circulation cells of stream lines are observed along primary diagonal for $\phi = 0^o$ (square cavity), one small roll of circulation appears near lower right corner then another comparatively large circulation roll appears near upper left corner and a big circulation roll of clockwise circulations appears between other two circulation rolls (see Figure 10 a). Whereas, when tilt angle ϕ is increased to 30^o and 45^o, circulations becomes symmetric about vertical axis passing through centre of bottom wall as seen in Figure 10 (b, c) and maximum height of circulation becomes 6.5 and 8 respectively.

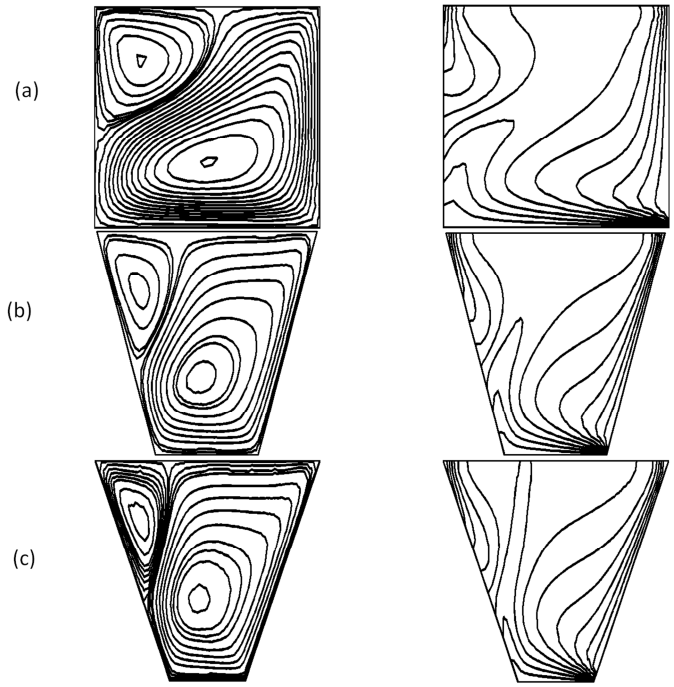

Figure 8. *Streamlines and Isotherms for cold right wall with* $Ra = 10^6, Pr = 10^3, Da = 10^{-3}$ *and* $Ha = 50$ *where (a)* $\phi = 0^o$ *(b)* $\phi = 30^o$ *(c)* $\phi = 45^o$.

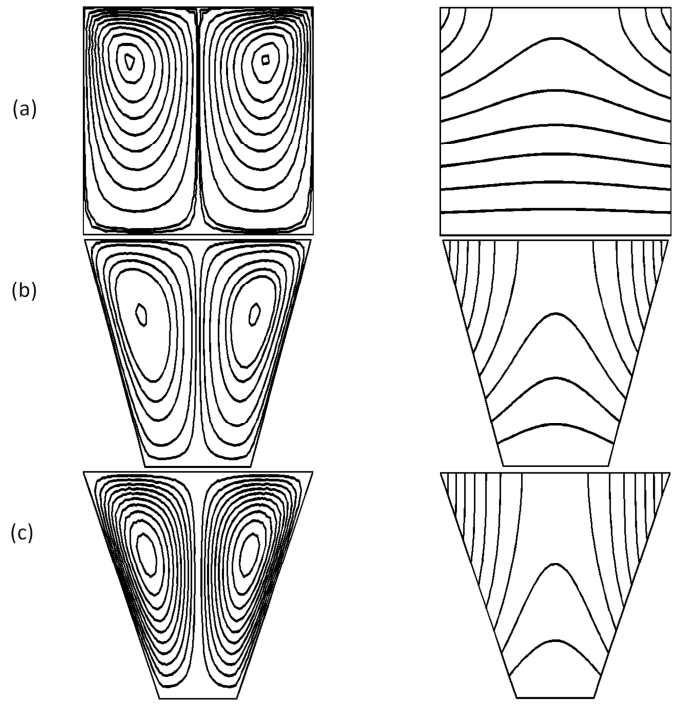

Figure 9. *Streamlines and Isotherms for linearly heated right wall with* $Ra = 10^6, Pr = 0.026, Da = 10^{-5}$ *and* $Ha = 50$ *where (a)* $\phi = 0^o$ *(b)* $\phi = 30^o$ *(c)* $\phi = 45^o$.

On the other hand isotherms are noted to be distorted and non-symmetric for $\phi = 0^o$ due to the convection dominant regime, where for $\theta \leq 0.5$ isotherms are broken up non-symmetrically to side walls as presented in Figure 10 (a). Afterwards, when tilt angle ϕ is increased, isotherms also become symmetric and isotherms are broken up symmetrically to side walls for $\theta \leq 0.7$ and $\theta \leq 0.8$ when $\phi = 30^o$ and $\phi = 45^o$respectively as seen in Figure 10 (b, c).

Figure 11, 12 illustrate isotherms and streamlines contour plots for $Ra = 10^6, Pr = 0.7, Da = 10^{-5} - 10^{-3}$ and $Ha = 50$. It is depicted in figures that, for sufficiently small Darcy number ($Da = 10^{-5}$) there are no prominent effects with increase in Prandtl while the magnitude of stream function becomes 0.085 for $\phi = 0^o$ (Figure 11 a), 0.18 for $\phi = 30^o$ (Figure 11 b) and 0.2 for $\phi = 45^o$ (Figure 11 c).

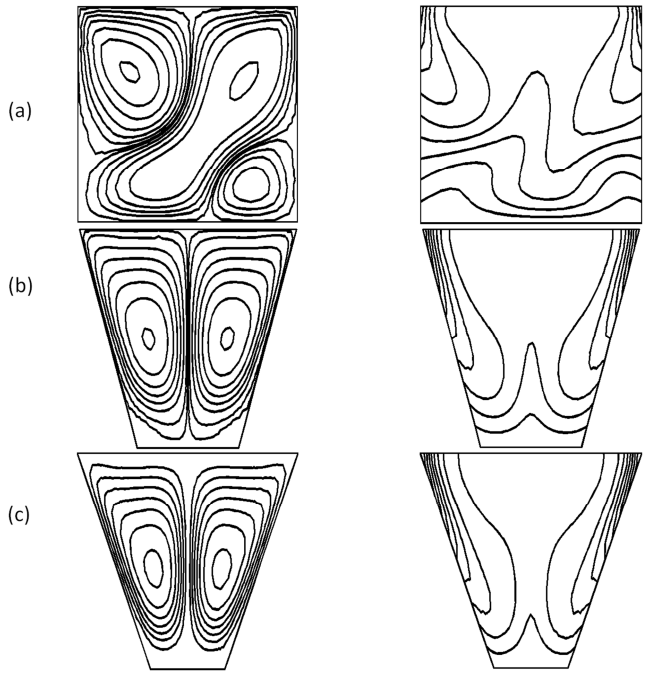

Figure 10. *Streamlines and Isotherms for linearly heated right wall with* $Ra = 10^6, Pr = 0.026, Da = 10^{-3}$ *and* $Ha = 50$ *where (a)* $\phi = 0^o$ *(b)* $\phi = 30^o$*(c)* $\phi = 45^o$.

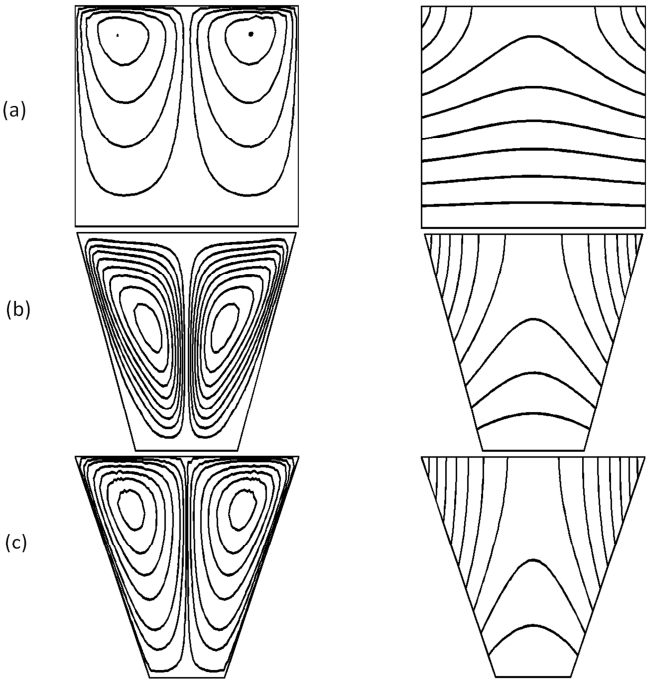

Figure 11. *Streamlines and Isotherms for linearly heated right wall with* $Ra = 10^6, Pr = 0.7, Da = 10^{-5}$ *and* $Ha = 10^3$ *where (a)* $\phi = 0^o$ *(b)* $\phi = 30^o$*(c)* $\phi = 45^o$.

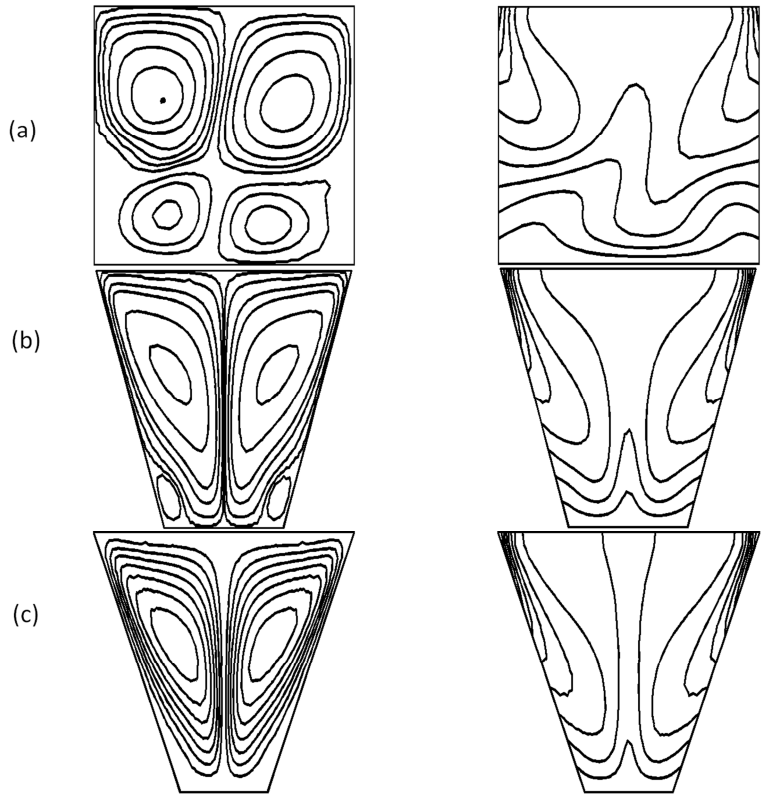

Figure 12. *Streamlines and Isotherms for linearly heated right wall with* $Ra = 10^6, Pr = 0.7, Da = 10^{-3}$ *and* $Ha = 50$ *where (a)* $\phi = 0^o$ *(b)* $\phi = 30^o$ *(c)* $\phi = 45^o$.

Whereas prominent effects of amplified Prandtl number may be seen when Darcy number is augmented to 10^{-3} as shown in Figure 12. With this escalation in Darcy number a pair of secondary circulations is observed near bottom wall for the inclinations of $\phi = 0^o$ and $\phi = 30^o$. The primary circulation cells are pushed upward by the secondary circulation cells because of strong convection near bottom wall as depicted in Figure 12 (a, b).

It is further observed that augmentation in tilt angle ϕ weakens secondary circulation and it disappears for $\phi = 45^o$ consequently streamlines are reduced into two rolls of circulations symmetric about vertical axis passing through centre of bottom line while maximum heights ($|\psi|_{\max}$) of streamlines becomes 4.7 for $\phi = 0^o$, 6.5 for $\phi = 30^o$and 8 for $\phi = 45^o$ respectively.

Furthermore, isotherms against small Darcy number ($Da = 10^{-5}$) are smooth and symmetric about vertical central line where, isotherm contours are symmetrically broken to side walls for $\theta \leq 0.3, \theta \leq 0.6$ and $\theta \leq 0.7$ when $\phi = 0^o, 30^o$ and 45^o respectively as shown in Figure 11. Whereas, when Darcy number is amplified to 10^{-3}, distorted isotherms are observed for $\theta \leq 0.5$ when $\phi = 0^o$ (see Figure 12 a) while, curves are mounted to opposite side walls near the lower region cavity and mounted upwards near centre of bottom wall as observed in Figure 12.

Figure 13, 14 shows the results for $Ra = 10^6, Pr = 10^3, Da = 10^{-5} - 10^{-3}$ and $Ha = 50$. It has been noticed that, when Prandtl number is magnified to 1000 and Darcy number is kept as small as 10^{-5}, the temperature and stream curves are pushed towards inclined walls where, stream contours appears as two rolls of clockwise and anti-clockwise circulations which are symmetric about vertical line passing through centre of bottom wall. The magnitude of stream function is 0.18 for $\phi = 0^o$, 0.3 for $\phi = 30^o$ and 0.28 for $\phi = 45^o$ respectively. Moreover, isotherms are found symmetric and monotonic showing dominance of conduction regime while all isotherm contours are seen broken in case of $\phi = 45^o$, whereas isotherms are noted to be broken when $\theta \leq 0.5$ for $\phi = 0^o$ and when $\theta \leq 0.8$ for $\phi = 30^o$ as expressed in Figure 13.

Increasing Darcy number to 10^{-3} results into secondary circulation near lower left and right corners when $\phi = 0^o$. This secondary circulation is weaker than that appeared for $Pr = 0.7$ in Figure 12 and it disappears in the cases when $\phi = 30^o$ and $\phi = 45^o$ resulting in two symmetric rolls of clockwise and anti-clockwise circulation. Maximum height of stream function is noted to be 7, 8, and 9 for $\phi = 0^o, \phi = 30^o$ and $\phi = 45^o$ respectively. On the other hand, non-monotonic distorted isotherm contours are observed in this case while, curves are symmetrically broken and clustered to side walls when $\theta \leq 0.7$ for $\phi = 0^o$ and when $\theta \leq 0.8$ for $\phi = 30^o$and $\phi = 45^o$ as shown in Figure 14.

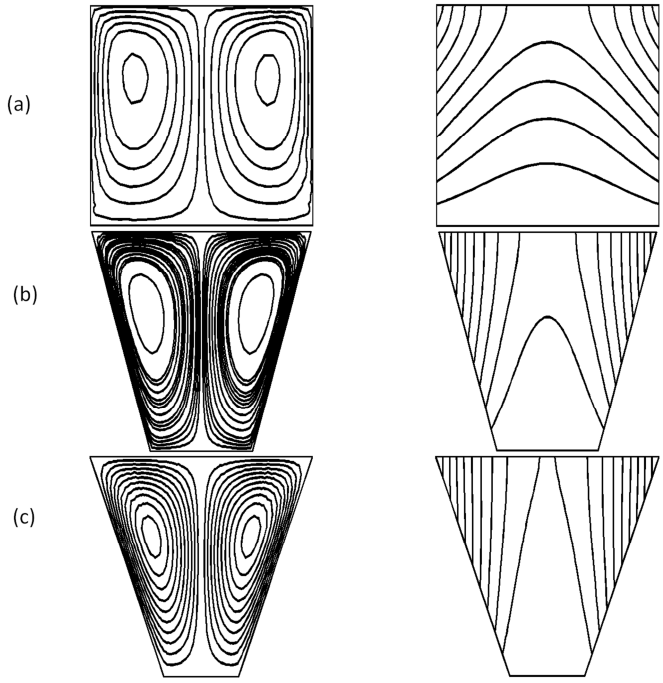

Figure 13. *Stream lines and Isotherms for linearly heated right wall with* $Ra = 10^6, Pr = 10^3, Da = 10^{-5}$ *and* $Ha = 50$ *where (a)* $\phi = 0^o$ *(b)* $\phi = 30^o$*(c)* $\phi = 45^o$.

Figure 15 contains plot of heat transfer rate in terms of local Nusselt number along uniformly heated bottom wall for the case of cold right wall. Curves are obtained for different values of Darcy number Da and Prandtl number Pr where, Rayleigh number Ra and Hartman number Ha are fixed to be $10^6$and 50 respectively.

It is observed that, Nu_b is 1 at left edge of bottom wall for all inclinations when $a = 10^{-5} - 10^{-3}$, this owes the fact that both walls intersection at bottom left corner node are at same temperature which is 1. Where, heat transfer rate is maximum at right edge of bottom wall due to the singularity appearing at this corner. It is also seen that, heat transfer rate accretes with distance and this increase becomes more rapid when we amplify the value of Darcy number Da from 10^{-5} to 10^{-3}. It is further observed that, when Pr is increased from 0.026 to 1000, heat transfer rate is depreciated for $Da = 10^{-5}$ and 10^{-4} but for $Da = 10^{-3}$, Nu_b escalates with distance up to 0.6 and then it is abates onward, while rate of depreciation is reduced with increase in tilt angle.

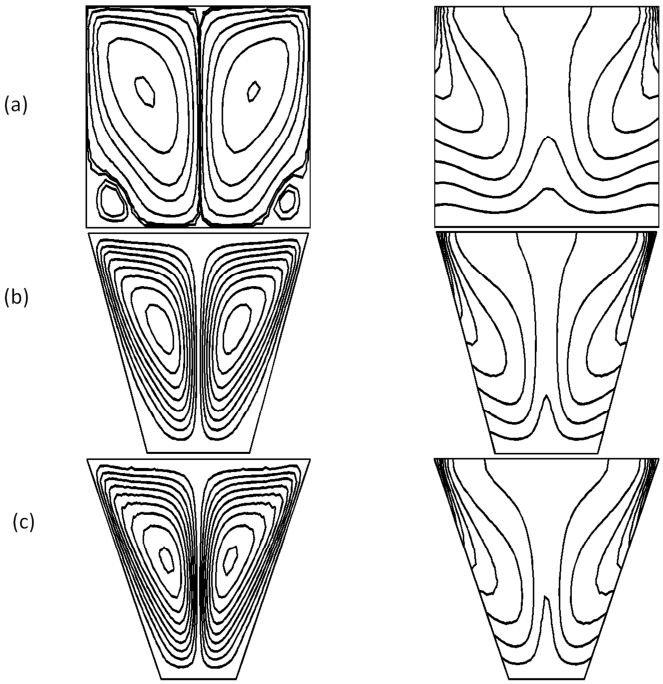

Figure 14. *Streamlines and Isotherms for linearly heated right wall with* $Ra = 10^6, Pr = 10^3, Da = 10^{-3}$ *and* $Ha = 50$ *where (a)* $\phi = 0^o$ *(b)* $\phi = 30^o$*(c)* $\phi = 45^o$.

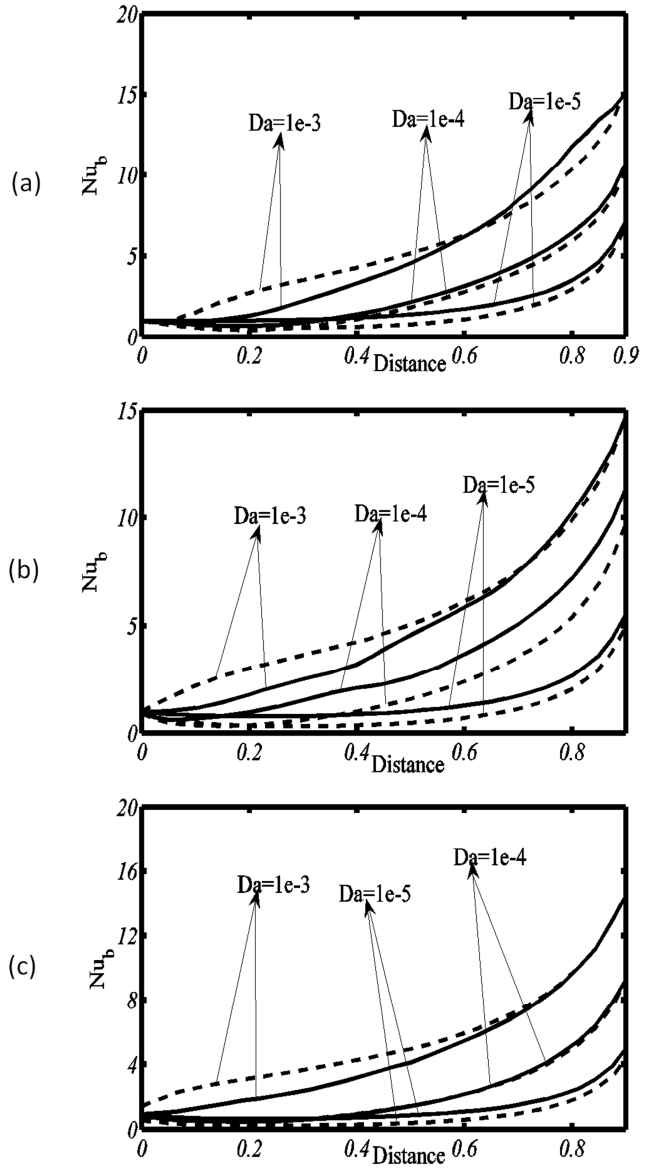

Figure 15. *Local Nusselt number for bottom wall with cold right wall considering* $Pr = 0.026$ *(solid lines) and* $Pr = 1000$ *(dotted lines) with* $Ra = 10^6$ *where (a)* $\phi = 0^o$ *(b)* $\phi = 30^o$ *(c)* $\phi = 45^o$.

Figure 16 shows local Nusselt number along linearly heated left wall for the case of cold right wall and it is observed that, for $Da = 10^{-5}$ and 10^{-4}, heat transfer rate along left wall Nu_l is almost parallel to x-axis for all tilt angles ϕ up to 0.8 and then increases up to upper left corner for $\phi = 0^o$ while, for $\phi = 30^o$ and $\phi = 45^o$ Nusselt number Nu_l increases up to 1.1 and 1.2 respectively and then decreases again afterwards (Figure 16 a, b, c). Where, for $Da = 10^{-3}$ and $Pr = 0.026$, Nu_l appears as sinusoidal wave due to varying temperature gradient while, for $Pr = 1000$, higher heat transfer rate is observed along left wall.

Figure 17 shows local Nusselt number for cold right wall and it is noticed that for $Da = 10^{-5}$ and 10^{-4}, local Nusselt number along right wall Nu_r abates sharply from 0 to 0.1 and augments afterwards at a very slow rate. Where for $Da = 10^{-3}$ with $Pr = 0.026$, Nu_r first declines from 0 to 0.1 in similar fashion but increases afterwards on a faster rate and when Pr is amplified to 1000 heat transfer rate remains same for $Da = 10^{-5}$ corresponding to all tilt angles and for $Da = 10^{-4}$ transfer rate decays for $\phi = 30^o$ and 45^o comparatively but for $\phi = 0^o$ it first decreases and then increases after 0.65 . Whereas, for $Da = 10^{-3}$, Nu_r diminishes up to 0.65 and then acceretes onwards for all tilt angles.

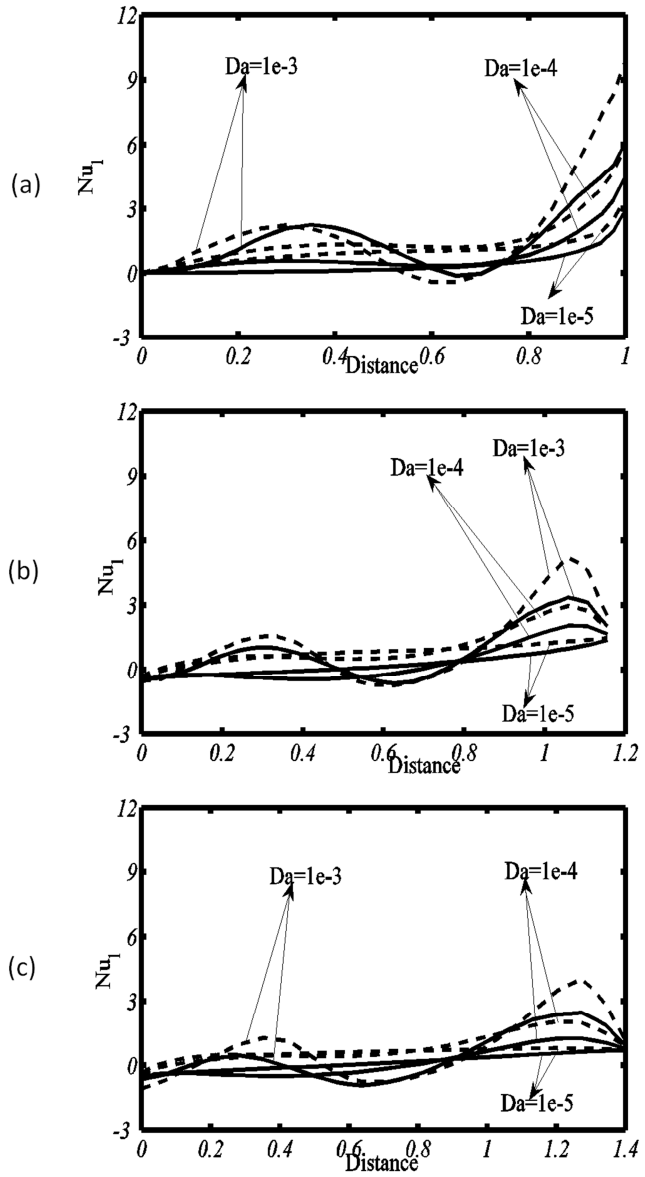

Figure 16. *Local Nusselt numbers for left wall with cold right wall considering* $Pr = 0.026$ *(solid lines) and* $Pr = 1000$ *(dotted lines) with* $Ra = 10^6$ *where (a)* $\phi = 0^o$ *(b)* $\phi = 30^o$ *(c)* $\phi = 45^o$.

Figures 18 and 19 correspond to case of linearly heated right wall. Figure 18 shows local Nusselt number for uniformly heated bottom wall. It is seen that for $Da = 10^{-5}$and 10^{-4}, local Nusselt number along bottom wall Nu_b decreases from 0 to 0.5 for both $Pr = 0.026$ and $Pr = 1000$ when tilt angle is $\phi = 30^o$and 45^o and rises after 0.5 up to 1 while, low heat transfer rate is observed for higher Prandtl

Number $Pr = 1000$. Whereas for $\phi = 0^o$, Nusselt number behave in a similar way as for other tilt angles when $Pr = 1000$ but for $Pr = 0.026$ curve of Nusselt number is almost parallel to x-axis corresponding to $Da = 10^{-5}$ while, for $Da = 10^{-4}$, Nu_b decays after increasing slightly and then again augments making a wave pattern. Furthermore, for $Da = 10^{-3}$, Nu_b first escalates from both corners (i.e. 0 and 0.1), afterwards it depreciates toward centre and a minima occurs at centre of x-axis while, two local maximums are seen in left and right half respectively. This pattern corresponds to the fact that the singularity from right bottom corner has been removed in this case and both walls are heated in same fashion. Similar behavior is observed for $Pr = 1000$ for all tilt angles.

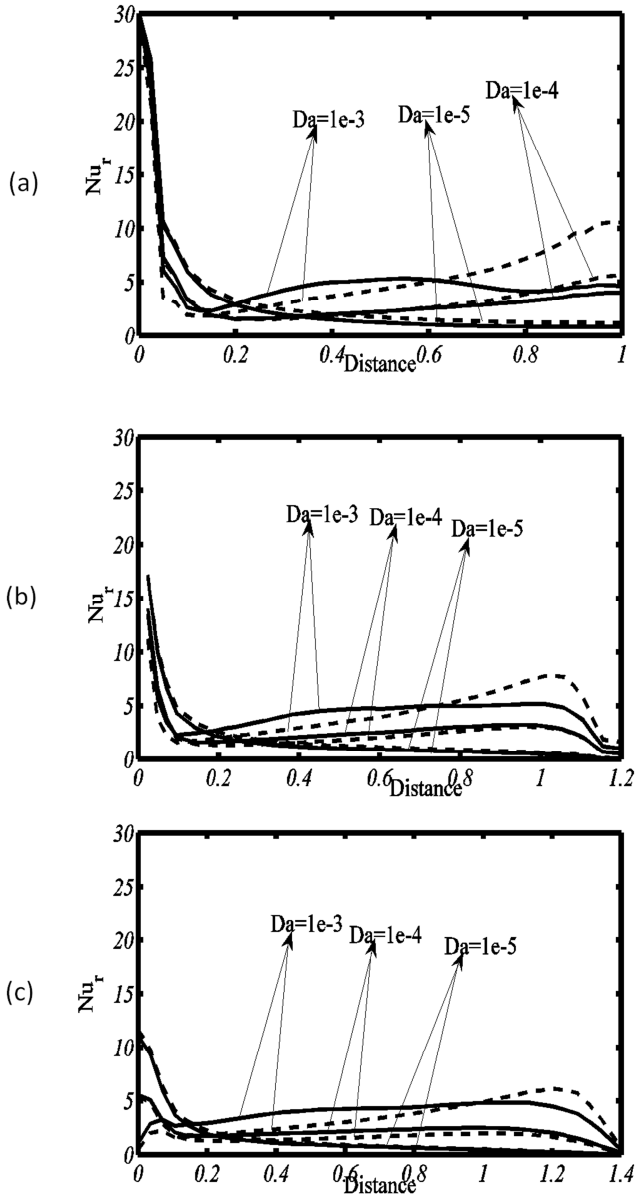

Figure 17. *Local Nusselt number for cold right wall considering* $Pr = 0.026$ *(solid lines) and* $Pr = 1000$ *(dotted lines) with* $Ra = 10^6$ *where (a)* $\phi = 0^o$ *(b)* $\phi = 30^o$ *(c)* $\phi = 45^o$.

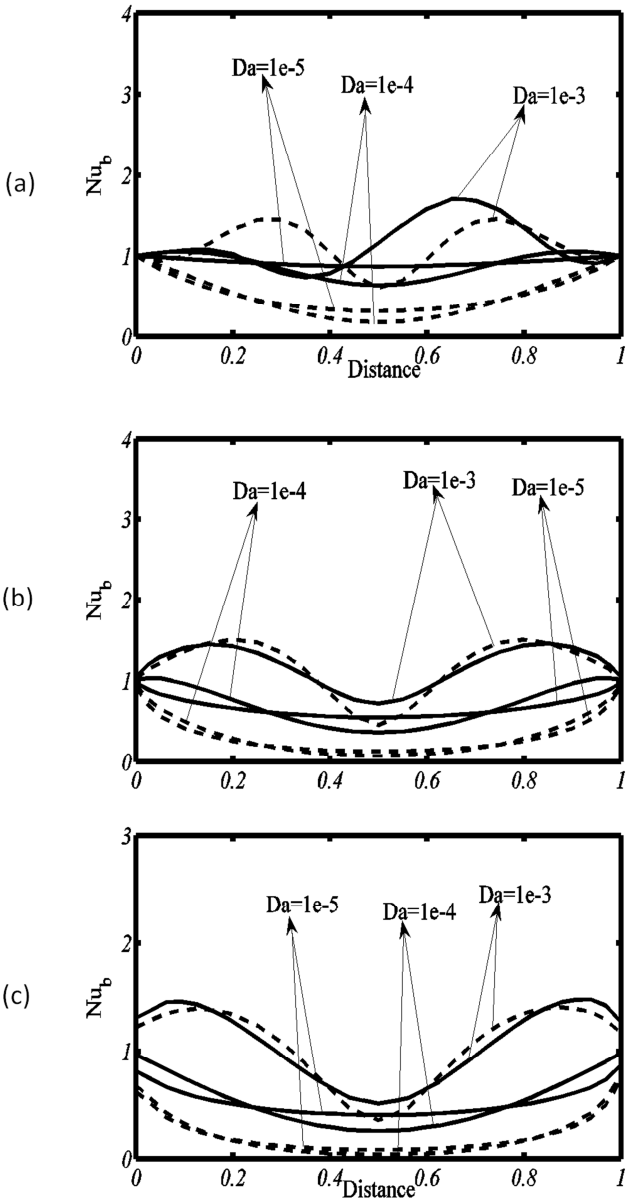

Figure 18. *Local Nusselt number for bottom wall with linearly heated right wall considering* $Pr = 0.026$ *(solid lines) and* $Pr = 1000$ *(dotted lines) with* $Ra = 10^6$ *where (a)* $\phi = 0^o$ *(b)* $\phi = 30^o$ *(c)* $\phi = 45^o$.

As both side walls are exposed to a similar heating profile therefore same curve for Nusselt number is obtained. Figure 19 shows local Nusselt number for linearly heated side walls. Curves are obtained for various values of Darcy number $Da = 10^{-5} - 10^{-3}$ and Prandtl number $Pr = 0.026 - 1000$ where Rayleigh number Ra and Hartman number Ha are kept fixed to be $10^6$and 50 respectively. It is observed that for $Da = 10^{-5}$ and 10^{-4}, local Nusselt number Nu_s along the side wall is almost parallel to x-axis up to 0.8 for all tilt angles ϕ and then increases afterwards sharply for $\phi = 0^o$ but for $\phi = 30^o$and 45^o, Nu_s amplifies slowly up to 1.1 and 1.2 respectively and then diminishes again afterwards as seen in Figure 19 (a, b, c). Whereas, for $Da = 10^{-3}$ and $Pr = 0.026$, Nu_s first decays from 0 to 0.55 then augments onwards for $\phi = 0^o$ but for $\phi = 30^o$and 45^o, it decreases a little, then escalates for majority of region and near the end it

depreciates again. While, for $Pr = 1000$ higher heat transfer rate is observed for all tilt angles and Darcy numbers.

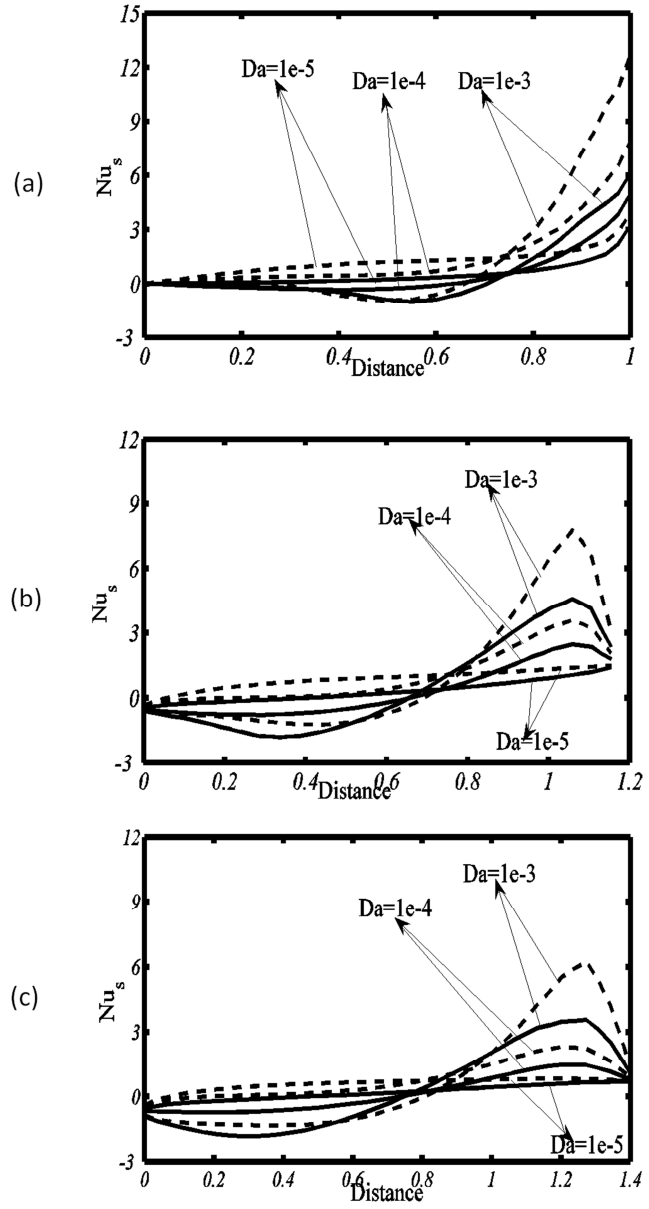

Figure 19. *Local Nusselt number for side walls when right wall is under linear heating considering* $Pr = 0.026$ *(solid lines) and* $Pr = 1000$ *(dotted lines) with* $Ra = 10^6$ *where (a)* $\phi = 0^o$ *(b)* $\phi = 30^o$*(c)* $\phi = 45^o$.

6. Conclusion

The numerical results of temperature distributions and the streamlines in a trapezoidal cavity with uniformly heated bottom wall in presence of MHD are analysed using Finite Element Method (FEM) for linearly heated or cold right wall. Equations governing flow problem are first simplified using penalty method to eliminate pressure term and then Gelarkin weighted residual technique is employed to reduce the governing eqution to a system of algebraic equations. The reduced algebraic equations are nonlinear requiring iterative technique to solve, hence Newtons Raphson method is applied to compute solution for wide range of physical parameters including Darcy number and Prandtl number.

In the case of cold right wall, It is observed that, for small Darcy number ($Da = 10^{-5}$) isotherms are smooth, monotonic but non-symmetric for all Prandtl numbers showing conduction dominant regime and in addition to primary clockwise circulation cell, a small secondary anti-clockwise circulation cell also appears in cavity. Increasing Prandtl number amplifies strength of secondary circulation while, augmentation in Darcy number ($Da = 10^{-3}$) also escalates the strength of both primary and secondary circulation where isotherms gets distorted with this magnification in Darcy number. On the other hand, two symmetric rolls of stream lines circulations and symmetric isotherms are observed for the case of linearly heated right wall. In this case also, smooth and monotonic isotherms are obtained for small Darcy number ($Da = 10^{-5}$) which gets distorted when Darcy number is mounted ($Da = 10^{-3}$) however, two rolls of secondary circulations are observed near bottom corners of cavity in addition to two primary roll where, these secondary circulations gets weaken with increase in tilt angle and vanishes completely for $\phi = 45^o$. Whereas, increasing Prandtl and Darcy number increases strength of circulation. It is further observed that, heat transfer rate along bottom wall Nu_b is maximum at right bottom corner for the case of cold right wall because of the singularity appearing at that edge. While along left wall, Nusselt number Nu_l is espied parallel to x-axis up to 0.8 for all inclination angles when $Da = 10^{-4}$ and 10^{-5} while for $Da = 10^{-3}$, curves for Nu_l appears like sinusoidal wave corresponding to case of cold right wall. It is also ascertained that in case of cold right wall, local Nusselt number along right wall Nu_r abates sharply from 0 to 0.1 and accretes afterwards at a very slow rate for $Da = 10^{-5}$ and 10^{-4}. Where for $Da = 10^{-3}$ with $Pr = 0.026$, Nu_r first diminishes from 0 to 0.1 and then escalates afterwards on a faster rate. When right wall is heated linearly, heat transfer rate Nu_b along bottom wall is found constant for $Pr = 0.026$ corresponding to $Da = 10^{-5}$ while, for $Da = 10^{-4}$, Nu_b declines after augmenting slightly and then again amplifies making a wave pattern. Furthermore, in the case of linearly heated right wall, local Nusselt number along the side wall Nu_s is almost parallel to x-axis up to 0.8 for all tilt angles ϕ and then it rises afterwards sharply for $\phi = 0^o$ but for $\phi = 30^o$ and 45^o, Nu_s increases slowly up to 1.1 and 1.2 respectively and then decreases again afterwards when $Da = 10^{-5}$ and 10^{-4}. Whereas, for $Da = 10^{-3}$ and $Pr = 0.026$, Nu_s first decreases from 0 to 0.55 then increases onwards for $\phi = 0^o$ but for $\phi = 45^o$ and $\phi = 30^o$ it diminishes a little, then increase for majority of region and near the end decreases again.

References

[1] T. Basak, S. Roy, A. Singh, A. R. Balakrishnan, Natural convection flows in porous trapezoidal enclosures with various inclination angles, International Journal of Heat and Mass Transfer 52 (2009) 4612–4623.

[2] Y. Varol, H. F. Oztop, I. Pop, Numerical analysis of natural convection for a porous rectangular enclosure with sinusoidally varying temperature profile on the bottom wall, International Communications in Heat and Mass Transfer 35 (2008) 56–64.

[3] A. Buan, D. Poulikakos, The nondarcy regime for vertical boundary layer natural convection in a porous medium, International Journal of Heat and Mass Transfer 27 (1984) 717–723.

[4] T. Basak, S. Roy, T. Paul, I. Pop, Natural convection in a square cavity filled with a porous medium: Effects of various thermal boundary conditions, International Journal of Heat and Mass Transfer 49 (2006) 1430–1441.

[5] X. B. Chen, P. Yu, S. H. Winoto, Free convection in a porous wavy cavity based on the darcy-brinkman-forchheimer extended model, Numerical Heat Transfer, Part A, 52 (2007): 377–397.

[6] T. Basak, S. Roy, A. Singh, B. D. Pandey, Natural convection flow simulation for various angles in a trapezoidal enclosure with linearly heated side wall(s), International Journal of Heat and Mass Transfer 52 (2009) 4413–4425.

[7] T. Basak, S. Roy, S. K. Singh, I. Pop, Finite element simulation of natural convection within porous trapezoidal enclosures for various inclination angles: Effect of various wall heating, International Journal of Heat and Mass Transfer 52 (2009) 4135–4150.

[8] R. Anandalakshmi, T. Basak, Heat flow visualization for natural convection in rhombic enclosures due to isothermal and non-isothermal heating at the bottom wall, International Journal of Heat and Mass Transfer 55 (2012) 1325–1342.

[9] S. A. Khashan, A. M. Al-Amiri, I. Pop, Numerical simulation of natural convection heat transfer in a porous cavity heated from below using a non-Darcian and thermal non-equilibrium model, International Journal of Heat and Mass Transfer 49 (2006) 1039–1049.

[10] D. Poulikakos, A. Bejan, The departure from Darcy flow in natural-convection in a vertical porous layer, Physics of Fluids 28 (1985) 3477–3484.

[11] A. A. Merrikh, A. A. Mohamad, Non-Darcy effects in buoyancy driven flows in an enclosure filled with vertically layered porous media, International Journal of Heat and Mass Transfer 45 (2002) 4305–4313.

[12] A. M. Al-Amiri, Natural convection in porous enclosures: the application of the two-energy equation model, Numerical Heat Transfer, Part A, 41 (2002): 817-834.

[13] G. Lauriat, V. Prasad, Non-Darcian effects on natural convection in a vertical porous enclosure, International Journal of Heat and Mass Transfer 32 (1989) 2135–2148.

[14] B. M. D. S. Miranda, N. K. Anand, Convective heat transfer in a channel with porous baffles, Numerical Heat Transfer, Part A, 46 (2004): 425–452.

[15] G. B. Kim, J. M. Hyun, H. S. Kwak, Buoyant convection in a square cavity partially filled with a heat-generating porous medium, Numerical Heat Transfer, Part A, 40 (2001): 601-618.

[16] T. Basak, S. Roy, A. Singh, I. Pop, Finite element simulation of natural convection flow in a trapezoidal enclosure filled with porous medium due to uniform and non-uniform heating, International Journal of Heat and Mass Transfer 52 (2009) 70–78.

[17] T. Basak, S. Roy, A. Singh, A. R. Balakrishnan, Natural convection flows in porous trapezoidal enclosures with various inclination angles, International Journal of Heat and Mass Transfer 52 (2009) 4612–4623.

[18] T. Basak, S. Roy, I. Pop, Heat flow analysis for natural convection within trapezoidal enclosures based on heatline concept, International Journal of Heat and Mass Transfer 52 (2009) 2471–2483.

[19] M. S. Hossain, M. A. Alim, MHD free convection within trapezoidal cavity with non uniform heated bottom wall, International Journal of Heat and Mass Transfer 69 (2014), 327-336.

[20] T. Basak, S. Roy, A. R. Balakrishnan, Effects of thermal boundary conditions on natural convection flow within a square cavity, International Journal of Heat and Mass Transfer 49 (2006): 4525-4535.

[21] M. K. Moaleemi, K. S. Jang, Prandtl number effects on laminar mixed convection heat transfer in a lid-drivrn cavity, International Journal of Heat and Mass Transfer 35 (1992) 1881-1892.

[22] S. Roy, T. Basak, Finite element analysis of natural convection flows in a square cavity with non-uniformly heated wall(s), International Journal of Engineering Science 43 (2005) 668-680.

[23] T. Basak, S. Roy, P. K. Sharma, I. Pop, Analysis of mixed convection flows within a square cavity with uniform and non uniform heating of bottom wall, International Jouranal of Thermal Science 48 (2009): 891-912.

[24] T. S. Lee, Computational and experimental studies of convective fluid motion and heat transfer in inclined non-rectangular enclosures, International Journal of Heat and Fluid Flow 5 (1984) 29–36.

[25] T. S. Lee, Numerical experiments with fluid convection in tilted non-rectangular enclosures, Numerical Heat Transfer: Part A: Applications: An International Journal of Computation and Methodology 19 (1991) 487–499.

[26] J. T. V. Eyden, T. H. V. Meer, K. Hanjalic, E. Biezen, J. Bruining, Double-diffusive natural convection in trapezoidal enclosures, Intrnational Journal of Heat and Mass Transfer 41 (1998) 1885–1898.

[27] Y. Hu, Y. He, C. Qi, B. Jiang, H. I. Schlaberg, Experimental and numerical study of natural convection in a square enclosure filled with nanofluid, International Journal of Heat and Mass Transfer 78 (2014) 380–392.

[28] N. Soares, A. R. Gaspar, P. Santos, J. J. Costa, Experimental study of the heat transfer through a vertical stack of rectangular cavities filled with phase change materials, Applied Energy 142 (2015) 192–205.

[29] G. Yang, Y. Huang, J. Wu, L. Zhang, G. Chen, R. Lv, A. Cai, Experimental study and numerical models assessment of turbulent mixed convection heat transfer in a vertical open cavity, Building and Environment 115 (2017) 91–103.

[30] H. F. Oztop, Y. Varol, A. Koca, M. Firat, Experimental and numerical analysis of buoyancy-induced flow in inclined triangular enclosures, International Communications in Heat and Mass Transfer 39 (2012) 1237–1244.

[31] C. L. Chen, Y. C. Chung, T. F. Lee, Experimental and numerical studies on periodic convection flow and heat transfer in a lid-driven arc-shape cavity, International Communications in Heat and Mass Transfer 39 (2012) 1563–1571.

[32] D. Spura, J. Lueckert, S. Schoene, U. Gampe, Concept development for the experimental investigation of forced convection heat transfer in circumferential cavities with variable geometry, International Journal of Thermal Sciences 96 (2015) 277–289.

[33] Z. G. Shen, S. Y. Wu, L. Xiao, D. L. Li, K. Wang, Experimental and numerical investigations of combined free convection and radiation heat transfer in an upward-facing cylindrical cavity, International Journal of Thermal Sciences 89 (2015) 314–326.

[34] P. H. Oosthuizen, D. Naylor, An introduction to convective heat transfer analysis, McGraw-Hill, International Edition, (1999).

[35] Z. Stelzer, D. Cébron, S. Miralles, S. Vantieghem, J. Noir, P. Scarfe, A. Jackson, Experimental and numerical study of electrically driven magnetohydrodynamic flow in a modified cylindrical annulus. I. Base flow, Physics of Fluids 27 (2015) 077101.

[36] P. A. Davidson, An Introduction to Magnetohydrodynamics, Cambridge University Press, Cambridge, (2001).

[37] T. Basak, K. G. Ayappa, Influence of internal convection during microwave thawing of cylinders, AIChE J. 47 (2001) 835–850.

[38] A. Asaithambi, Numerical solution of the Falkner–Skan equation using piecewise linear functions, Appl. Math. Comput. 81 (2003) 607–614.

[39] J. N. Reddy, An Introduction to the Finite Element Method, McGraw-Hill, New York, 1993.

[40] M. M. Ganzarollli, L. F. Milanez, Natural convection in rectangular enclosure heated from below and symmetrically cooled from sides, International Journal of Heat and Mass Transfer 38: (1995), 1063-1073.